Improved global maps and 54-year history of wind-work on ocean inertial motions

Matthew H. Alford

Applied Physics Laboratory and School of Oceanography, University of Washington, Seattle, Washington, USA

Received 15 November 2002; accepted 6 February 2003; published 18 April 2003.

[1] The global distribution and 54-year time dependence of the energy-flux from the wind to near-inertial motions is computed by driving a slab mixed-layer model with NCEP/NCAR Reanalysis winds, improving upon previous estimates [*Alford*, 2001; *Watanabe and Hibiya*, 2002]. The slab model is solved spectrally with frequency-dependent damping. The resulting solutions are more physically sensible than the previous, and more skillful at high latitudes, where the inertial frequency approaches the 4×-daily sampling of the Reanalysis winds. This enables Alford's calculation, whose domain was limited to ±50°, to be extended to the poles. The high-latitude reliability is demonstrated by direct comparison with a high-resolution regional model (REMO) in the NE Atlantic. The total power input, 0.47 TW, has increased by 25% since 1948, paralleling observed increases in extratropical cyclone frequency and intensity. If believable, the trend may have important consequences for modulation of the meridional overturning circulation. *INDEX TERMS:* 4544 Oceanography: Physical: Internal and inertial waves; 4504 Oceanography: Physical: Air/sea interactions (0312); 4568 Oceanography: Physical: Turbulence, diffusion, and mixing processes; 4215 Oceanography: General: Climate and interannual variability (3309). **Citation:** Alford, M. H., Improved global maps and 54-year history of wind-work on ocean inertial motions, *Geophys. Res. Lett.*, *30*(8), 1424, doi:10.1029/2002GL016614, 2003.

1. Introduction

[2] The wind blowing on the sea surface generates mixed-layer currents rotating at the local inertial frequency that can force downward- and equatorward-propagating near-inertial waves. It has been suggested [*Munk and Wunsch*, 1998] that these, together with the tides [*Egbert and Ray*, 2002] and wind-work at lower frequencies [*Wunsch*, 1998], may provide enough power to maintain the deep ocean's stratification against the upwelling of cold water originating from the poles. Mapping each internal-wave source [*Egbert and Ray*, 2000; *Alford*, 2001] and subsequent propagation [*Alford*, 2003] is a first step toward a spatial map of internal-wave dissipation. Such a map would be a significant achievement, not only since this mixing may determine the strength of the meridional overturning circulation (MOC) [*Munk and Wunsch*, 1998], but also since climate models are sensitive to both the magnitude and distribution of mixing [*Samelson*, 1998]. Here, the focus is on the near-inertial source term.

[3] *D'Asaro* [1985] first computed the flux from the wind to inertial motions using buoy wind data to drive a local slab mixed-layer model [*Pollard and Millard*, 1970],

$$\frac{dZ}{dt} + (r + if)Z = \frac{T}{H}, \tag{1}$$

where $Z = u + iv$ is the mixed-layer current, $T = \rho^{-1}(\tau_x + i\tau_y)$ is the wind stress, H is the mixed-layer depth (MLD), and f is the inertial frequency. The damping coefficient, r, models the decay by propagation of the near-inertial motions. D'Asaro showed that wintertime storms were responsible for much of the mid-latitude forcing. Using NCEP/NCAR reanalysis winds (2.5° resolution, 4x-daily output) [*Kalnay et al.*, 1996], *Alford* [2001, hereinafter referred to as A01] produced spatial maps of this flux, which demonstrated broad western-intensified midlatitude maxima during local winter, and a total power input of 0.3 TW. Based on comparisons with 14 buoys between 40–60°N, A01 restricted his domain to ±50°, since solutions poleward of there were unreliable.

[4] *Watanabe and Hibiya* [2002, hereinafter referred to as WH] repeated the calculation with a similar wind product, extending the calculation to the poles. They obtained a global total over twice that of A01, attributing the difference to A01's neglect of a term in the expression for the flux. Here it is shown that the term, which is of order $r/f \ll 1$ (the same as the model accuracy), yields negligible differences, and that the A01 value was correct for the domain ±50°. Instead, several serious errors (Appendix A) in the WH calculation bias their estimate high.

[5] Here, improved estimates are obtained by solving equation (1) spectrally. A frequency-dependent damping $r(\sigma)$ is used that goes to zero for $\sigma < f$, where no wave propagation is permitted. By comparing the results to a high-resolution regional atmospheric model in the North Atlantic, A01's calculation can confidently be extended to the poles. This work presents these results, which are qualitatively similar to A01, but the improved model, the global coverage and the verification of the high-latitude solutions provide greater quantitative certainty. Finally, the flux is evaluated for the entire 54-year span of the NCEP/NCAR Reanalysis, and implications for the long-term variability of the MOC are discussed.

2. Comparison of Previous Results

2.1. Method

[6] The solution to (1) is well known, and may be viewed as the sum of a time-varying Ekman transport $Z_E = T/(r + if)H$ and an inertially rotating current, $Z_I \equiv Z - Z_E$, which is the solution to

$$\frac{dZ_I}{dt} = -(r + if)Z_I - \frac{1}{r + if}\frac{d(T/H)}{dt}. \tag{2}$$

0094-8276/03/2002GL016614$05.00

The flux into these inertial motions is given [*D'Asaro*, 1985] by

$$\Pi(H) = -Re\left[\rho \frac{Z_I}{(r-if)H}\frac{dT^*}{dt}\right]. \quad (3)$$

A more physically intuitive approximation to (3) is given by the vector product of the wind with the inertial current,

$$\hat{\Pi}(H) = Re[\rho Z_I T^*], \quad (4)$$

which neglects a term of order r/f, the same as the model accuracy. (This is shown by integrating (3) by parts (T. Hibiya, personal communication).)

[7] Both A01 and WH solved (2) for Z_I and then obtained the flux (A01 using (4), WH using (3)) for a reference MLD. The *Levitus and Boyer* [1994] climatology was then used to estimate H(x,t) and thence Π. A monthly ice-mask climatology [*da Silva et al.*, 1994], unnecessary for A01's ± 50° domain, and neglected by WH, is used here to exclude ice-covered regions.

2.2. Comparisons

[8] WH obtained a global total over twice A01, and argued that use of (4) instead of (3) biased A01's estimate low. To address this issue, the mean flux is evaluated using both methods for 1989–1995, the same years used by WH. The zonal-mean profile (Figure 1) indicates that (4) is a 25% overestimate (order r/f, the accuracy of the model itself) at high latitudes and a 25% underestimate at low latitudes. The high- and low-latitude differences nearly cancel, leading to less than 8% difference in the global totals. Neither the seasonal cycle, statistics, basin-by-basin distribution, nor global totals from A01 is changed by more than 10%. Instead, WH's high value results from several errors in their calculation (Appendix A).

3. The Spectral Solution

[9] Both previous solutions have two shortcomings: 1) the damping, r, is meant to model the decay of the mixed-layer motions due to wave propagation, which only occurs at rotary frequencies $|\sigma| > f$. Consequently, a frequency-dependent damping r(σ) that goes to zero for $|\sigma| < f$ is more appropriate. 2) The time-dependent Ekman solutions, Z_E, have variance in the inertial band, which are available for propagation but neglected in the previous solutions. Thus, the appropriate expression for the flux is

$$\Pi(H) = Re[\rho Z T^*], \quad (5)$$

where Z is the solution to (1) with a frequency-dependent damping coefficient,

$$r(\sigma) = r_o\left(1 - e^{-\sigma^2/2\sigma_c^2}\right), \quad (6)$$

where r_o = 0.15f as in A01, but here decays to zero for values $\sigma < \sigma_c \equiv f/2$. ($\sigma_c$ is the frequency below which the response is all "Ekman." Choosing $\sigma_c = 0$ causes the fluxes from (5) to be double the frequency-independent inertial-only case, but for a wide range around $\sigma_c = f/2$, the fluxes are only modestly enhanced (∼20–30%), with a weak dependence on σ_c. Importantly, results are not sensitive to the magnitude or functional form of (6), provided $r \ll f$.)

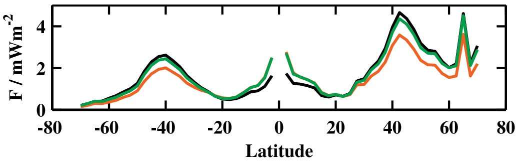

Figure 1. The zonal-mean flux averaged over the years 1989–1995. Black, red and green profiles are computed using equation (4), (3) and (5), respectively.

[10] Time-domain solutions to (1) are now impossible, but a spectral solution is straightforward since the transfer function, $R \equiv Z(\sigma)/T(\sigma)$, to (1) is simply

$$R(\sigma) = \frac{1}{H}\frac{r - i(f+\sigma)}{r^2 + (f+\sigma)^2}, \quad (7)$$

which again has an Ekman component,

$$R_E(\sigma) = \frac{1}{H}\frac{r - if}{r^2 + f^2} \quad (8)$$

and an inertial component, $R_I = R - R_E$.

[11] Solutions are obtained at each location by interpolating the 4×-daily wind-stress time series for each year onto a 65,536-point grid, Fourier transforming the wind time series to obtain $T(\sigma)$, applying the transfer function (7) to obtain $Z(\sigma) = R(\sigma)\, T(\sigma)$, and transforming back.

[12] The flux response Re[R(σ)] (Figure 2) is strongly peaked at $\sigma = -f$. With frequency-independent r, (1) (thin black) has a finite response at σ = 0 (the Ekman component, red), which in previous studies was subtracted to isolate the inertial response (thin green line). In the new variably-damped solutions, the "total" solution (7) is used (heavy black), whose zero-frequency response is now zero since r(σ = 0) = 0, but the inertial-band Ekman response is properly included. The phase of the resulting Z(t) are not noticeably affected, but the fluxes are accordingly slightly larger. The spectral solution also performs better at poor temporal resolution, allowing extension of the A01 domain to the poles (next section).

4. High-Latitude Response

[13] As latitude increases, f approaches the Nyquist frequency (2 cpd) of the NCEP winds. The effect on the resultant fluxes is ascertained by direct comparison with a high-resolution regional atmospheric model of the NE Atlantic [*Feser et al.*, 2001] (REMO) which uses the NCEP winds as its SW boundary condition. Since the REMO winds are output hourly at 0.5° resolution, they are not subject to temporal resolution issues and hence are an ideal benchmark. Here, the flux is computed using both NCEP and REMO winds (Figure 3a,b). (The NCEP and REMO winds are highly coherent at all frequencies over the entire domain. However, the spectra of the REMO winds at f are lower than the NCEP winds by a constant factor. To account for this attenuation, the REMO winds are multiplied by 1.32.) The visual correspondence is obvious, but the NCEP fluxes are attenuated at high latitude due to their 6-hour sampling.

[14] The zonal-mean flux from each is computed (Figure 3c), excluding the southwestern edge where the REMO winds are relaxed to the NCEP winds. The zonal-mean ratio (Figure 3d) indicates that little attenuation occurs south of 40°, decreasing to about 0.5 at 70°. A linear fit (heavy line)

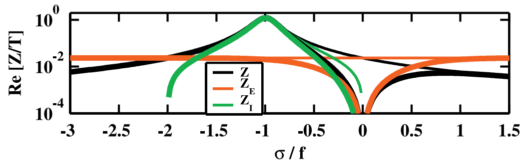

Figure 2. Flux transfer functions Re[R(σ)] for Z (black), Z_E (red) and Z_I (green) for the frequency-independent-r case (thin) and an r that decays to zero for $\sigma < 0.5f$ (thick).

is used here to correct the NCEP fluxes in both hemispheres. The REMO and corrected NCEP fluxes agree well at all latitudes (Figure 3e). Since this factor also works well with NE Pacific NCEP/buoy comparisons (not shown), the northern fluxes presented here are considered reliable. (The data-poor high-southern-latitude NCEP winds are less so, allowing the possibility that the fluxes there are underestimated.)

5. Results

5.1. Spatial Maps

[15] Seasonally-averaged spatial maps of the spectral-solution flux (Figure 4) are qualitatively identical to those presented in A01, and the reader is referred there for more details. As in A01, strong western-enhanced, midlatitude fluxes are observed with maxima in local winter associated with travelling storms. These midlatitude maxima are evident, as before, in the zonal-mean profile (Figure 1, green).

[16] The global power input from the wind to inertial motions is given by the area integral of the panels in Figure 4. For the period 1989–1995 (considered by WH), the mean input is 0.47 TW, about 60% higher than A01's previous estimate (owing to the larger domain and the incorporation of near-inertial Ekman motions), but only 70% of the WH value (see Appendix A).

5.2. 54-Year Record

[17] Since the 1950's the frequency and intensity of extratropical cyclones has increased in both the northern [*Graham and Diaz*, 2001] and southern [*Hopkins and Holland*, 1997] Pacific. The effects of these changes on the fluxes are investigated by computing the wind-work for each year of the NCEP Reanalysis, from 1948–2001. (The same MLD climatology is used for all years. However, wind, rather than MLD, fluctuations dominate the fluxes [A01].) The tropical input ($|lat| < 20°$) has remained nearly constant at 0.15 TW over the 54-year record (Figure 5, blue line), but the extratropical input has increased by about 40%. The total has increased about 25% over the 54 years, paralleling observations of increasing cyclone frequency (gray line), maximum wind, and wave heights in the North Pacific

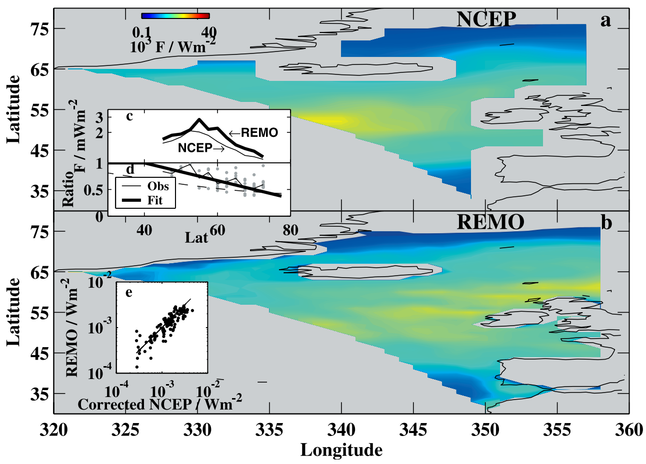

Figure 3. Annual-mean flux for 1988 from NCEP (a) and REMO (b). (c) The zonal-mean flux from the NCEP (thin) and REMO (thick) winds. (d) The ratio at each location (dots), the zonal mean (thin), a fit (thick), and the factor used by WH (dashed). (e) Scatter plot of REMO vs. corrected NCEP fluxes.

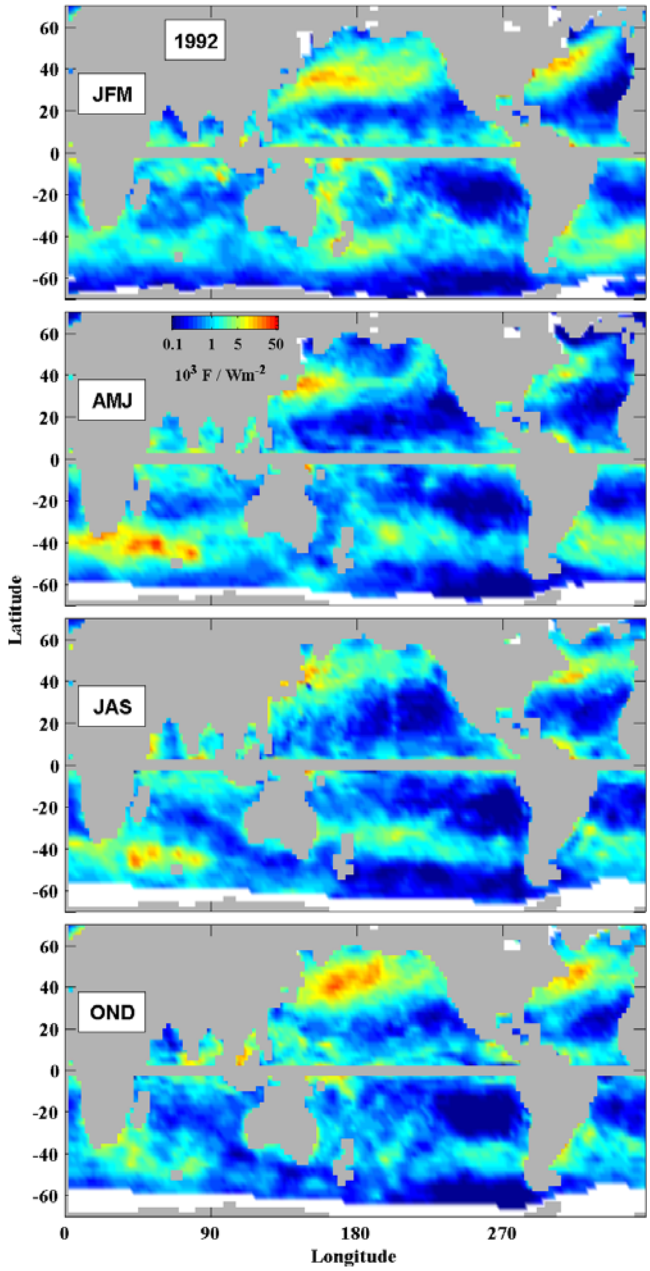

Figure 4. The 1992 global distribution of work done by the wind on near-inertial motions computed using (5) and incorporating monthly mixed-layer-depth variations. Each panel is a seasonal average over the months indicated at left. Ice is indicated in white.

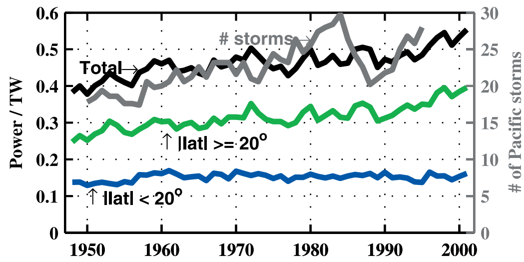

Figure 5. Time series from 1948–2001 of global dissipation due to near-inertial wind work integrated over the region equatorward (blue) and poleward (green) of 20°, and the total (black). Gray is the 5-year-running-mean number of North Pacific cyclones [*Graham and Diaz*, 2001].

[*Graham and Diaz*, 2001]. In addition, northern extratropical flux and cyclone frequency are coherent at 95% confidence at 10-year time scales. As expected, increased extratropical storminess results in greater inertial forcing. (The NCEP Reanalysis maintains the same assimilation scheme over time. However, differences in data techniques, coverage and processing over time can lead to spurious trends. Eliminating this possibility is not attempted here. However, *Graham and Diaz* [2001] compared NCEP Reanalysis winds with data from COADS and independent radiosondes and concluded that they were bias-free in the N. Pac.)

6. Conclusions

[18] The global total power input from 1989–1995 is 0.47 TW, comparable to estimates of the power converted from surface to internal tides [*Egbert and Ray*, 2002] (0.7 TW for M_2] and the work done by the wind on the general circulation [*Wunsch*, 1998] (≈1 TW). *Munk and Wunsch* [1998] have suggested that 2 TW of power are required to warm the cold, sinking leg of the meridional overturning circulation so that it can upwell. (It has been suggested that Ekman suction in the Southern Ocean could reduce this value to as low as 0.6 TW [*Webb and Suginohara*, 2001].) It appears that the wind and the tides together are sufficient to provide this power, contributing comparably.

[19] If abyssal mixing in fact throttles the MOC, then the observed secular increase in both the structure and magnitude wind-work would be accompanied by a strengthened MOC (if all else remained the same). The suggestion that long-term secular trends in energy available for small-scale mixing may affect the global climate underscores the need to understand rather than simply parameterize these processes: one space- and time-independent diffusivity value will clearly not suffice.

Appendix A: Errors in WH

[20] WH obtained a global total power input of 0.7 TW, over twice A01's ± 50° total. Their larger domain cannot account for all of the difference, since the present values, which are global and include the inertial-Ekman flux not accounted for by WH, are 30% lower than WH. Since A01's use of (4) results in negligible differences (section 2.2), it is suggested that three aspects of the WH calculation conspire to bias their estimate high.

[21] First, WH used a global-constant r = 0.25 cpd. Consequently, as f decreases at low latitude, r/f increases, violating the model assumption of $r \ll f$. For r = 0.25 cpd, r/f > 0.5 for latitudes <15°; this is 30% of the oceans. (A01's use of the more physical r = 0.15f avoids this problem). Aside from the questionable practice of solving a model whose assumptions are violated, overdamping may account for WH's large low-latitude fluxes.

[22] Second, WH extended their calculation to the poles without comparing with real data, in contrast to here and in A01. They also divided by an (untested) high-latitude correction factor attempting to account for the under-resolution of fluxes due to inadequate temporal sampling. This factor is substantially lower than that obtained directly here (Figure 3d). Applying the WH factor instead of the one used here magnifies the totals by 50%.

[23] Finally, WH counted all fluxes regardless of ice coverage, leading to high-latitude overestimates in some seasons. For example, one of their largest computed fluxes occurs south of 60°S in Sep–Nov (their Figure 4), when the region is climatologically covered in ice (Figure 4).

[24] **Acknowledgments.** This work was funded by the Office of Naval Research Young Investigator award, grant #N00014-02-1-0526. I thank Chris Garrett and Eric D'Asaro for discussions that led to the $r(\sigma)$ solutions.

References

Alford, M. H., Internal swell generation: The spatial distribution of energy flux from the wind to mixed-layer near-inertial motions, *J. Phys. Oceanogr.*, *31*, 2359–2368, 2001.
Alford, M. H., Energy available for ocean mixing redistributed by long-range internal-wave propagation, *Nature*, in press, 2003.
D'Asaro, E., The energy flux from the wind to near-inertial motions in the mixed layer, *J. Phys. Oceanogr.*, *15*, 943–959, 1985.
da Silva, A. M., C. C. Young, and S. Levitus, *Atlas of Surface Marine Data 1994*, vol. 2, *Anomalies of Directly Observed Quantities, NOAA Atlas NESDIS*, vol. 7, 83 pp., Natl. Oceanic and Atmos. Admin., Silver Spring, Md., 1994.
Egbert, G. D., and R. D. Ray, Significant dissipation of tidal energy in the deep ocean inferred from satellite altimeter data, *Nature*, *45*, 775–778, 2000.
Feser, F., R. Weisse, and H. von Storch, Multi-decadal atmospheric modeling for Europe yields multi-purpose data, *Eos Trans. AGU*, *82*, 305–311, 2001.
Graham, N., and H. Diaz, Evidence for intensification of North Pacific winter cyclones since 1948, *J. Clim*, *82*, 1869–1893, 2001.
Hopkins, L., and G. Holland, Australian heavy-rain days and associated east coast cyclones: 1958–92, *J. Clim.*, *10*, 621–636, 1997.
Kalnay, E. M., et al., The NCEP/NCAR 40-year reanalysis project, *Bull. Am. Meteorol. Soc.*, *77*, 437–471, 1996.
Levitus, S., and T. Boyer, *World Ocean Atlas 1994*, vol. 4, *Temperature, NOAA Atlas NESDIS*, vol. 4, 129 pp., Natl. Oceanic and Atmos. Org., Silver Spring, 1994.
Munk, W., and C. Wunsch, Abyssal recipes II: Energetics of tidal and wind mixing, *Deep Sea Res., Part I*, *45*, 1977–2010, 1998.
Pollard, R. T., and R. C. Millard, Comparison between observed and simulated wind-generated inertial oscillations, *Deep Sea Res.*, *17*, 153–175, 1970.
Samelson, R. M., Large scale circulation with locally enhanced vertical mixing, *J. Phys. Oceanogr.*, *28*, 712–726, 1998.
Watanabe, M., and T. Hibiya, Global estimates of the wind-induced energy flux to inertial motions in the surface mixed layer, *Geophys. Res. Lett.*, *29*(8), 1239, doi:10.1029/2001GL014422, 2002.
Webb, D. J., and N. Suginohara, Vertical mixing in the ocean, *Nature*, *409*, 37, 2001.
Wunsch, C., The work done by the wind on the oceanic general circulation, *J. Phys. Oceanogr.*, *28*, 2332–2340, 1998.

M. Alford, Applied Physics Laboratory, 1013 NE 40th St Seattle, WA 98105, USA. (malford@apl.washington.edu)